

Spin waves in bilayers of transition-metal dichalcogenides

Wojciech Rudziński^{1,*}, Józef Barnaś^{1,2}, and Anna Dyrdał¹

¹*Faculty of Physics, Adam Mickiewicz University in Poznań,
ul. Uniwersytetu Poznańskiego 2, 61-614 Poznań, Poland and*

²*Institute of Molecular Physics, Polish Academy of Sciences,
ul. M. Smoluchowskiego 17, 60-179 Poznań, Poland*

(Dated: November 21, 2023)

Van der Waals magnetic materials are currently of great interest as materials for applications in future ultrathin nanoelectronics and nanospintronics. Due to weak coupling between individual monolayers, these materials can be easily obtained in the monolayer and bilayer forms. The latter are of specific interest as they may be considered as natural two-dimensional spin valves. In this paper, we study theoretically spin waves in bilayers of transition metal dichalcogenides. The considerations are carried within the general spin wave theory based on effective spin Hamiltonian and Hollstein-Primakoff-Bogolubov transformation. The spin Hamiltonian includes intra-layer as well as inter-layer nearest-neighbour exchange interactions, easy-plane anisotropy, and additionally a weak in-plane easy-axis anisotropy. The bilayer systems consist of two ferromagnetic (in-plane magnetization) monolayers that are coupled either ferromagnetically or antiferromagnetically. In the latter case, we analyse the spin wave spectra in all magnetic phases, i.e. in the antiferromagnetic, spin-flop, and ferromagnetic ones.

I. INTRODUCTION

Two-dimensional (2D) van-der-Waals magnetic materials are currently of great interest due to expected applications in atomically-thin spintronics devices, like for instance spin valves, memory elements, and others [1–4]. In the bulk form, these materials are build of monolayers that are weakly coupled by van-der-Waals forces. Therefore, it is relatively easy to obtain them in the form of thin films with arbitrary number of monolayers, down to bilayers and single monolayers. Accordingly, magnetic ordering and magnetic properties of van der Waals materials depend on the number of coupled monolayers.

Expected applications of 2D magnetic materials stimulated also intensive theoretical investigations of their physical properties as well as search for new materials with better characteristics, especially with higher Curie/Neel temperatures. Of particular interest are their electronic and magnetic properties, including also spin dynamics and spin wave propagation [5–11].

Magnetic ground state of van der Waals materials can be relatively easily tuned by external strain or gating [12–15]. These properties, together with strong magnetoresistance effects, magneto-optical properties, spin-filtering, spin-to-charge interconversion, and topological (electronic and magnon) transport make these materials extremely attractive not only for applications but also for theoretical studies. Moreover, magnetic van-der-Waals structures also offer unique possibilities for tuning magnetic anisotropy [16], which is crucial for various applications where magnetic anisotropy plays an active role. Magnetic anisotropy also allows to overcome large spin

fluctuations in 2D systems and therefore facilitates stabilization of the spin structure. Interestingly, such a tuning of magnetic anisotropy in van der Waals materials can be easily achieved with chemical doping, externally-induced strains, or proximity effects [1].

Various groups of magnetic van der Waals materials are currently known. These materials have also various physical and especially transport properties, including ferromagnetic semiconductors, e.g. VS_2 , VSe_2 [17–21], itinerant ferromagnets such as Fe_3GeTe_2 [2, 22], and insulating ferromagnets like CrI_3 [23] or $\text{Cr}_2\text{Ge}_2\text{Te}_6$ [1, 24]. In this paper we focus on magnetic properties and especially on spin wave excitations in a specific group of ferromagnetic 2D van der Waals materials, i.e. in transition-metal dichalcogenides (TMDs) [25–28], MX_2 , where M stands for a transition metal atom and X for a chalcogen one (X=S, Se, Te). These materials have Curie temperatures in the vicinity of room temperature, so they are of certain potential for practical applications. We also note that spin wave excitations in van der Waals structures are currently of great interest for magnonics applications, and have been studied theoretically as well as experimentally in various materials, including TMDs, chromium trihalides (CrI_3 , CrCl_3) and others. It has been shown, for instance, that spin waves in chromium trihalides have features that follow from topological properties of these materials [8, 9]. Such topologically-induced features also occur in TMDs [29–31].

A specific subgroup of TMDs are Vanadium-based dichalcogenides, VX_2 with X=S, Se and Te [17–21, 25–27]. Two different polymorphs of VX_2 materials are currently known, i.e. the trigonal prismatic crystallographic structure (shortly referred to in the following as the H phase) and the octahedral structure (referred to as the T phase) [25–27]. An individual monolayer of these materials consists of a hexagonal atomic plane of Vanadium

* wojrudz@amu.edu.pl

atoms, sandwiched between two chalcogen (X) atomic planes. In-plane positions of the chalcogen atoms in these two planes are the same (one on the other) in the T phase but these planes are rotated by some angle in the H phase. Experimental and theoretical studies reveal a metal-insulator transition [18] when reducing thickness of VSe₂ layers down to a 2D monolayer. In turn, the intrinsic ferromagnetism in the VSe₂ monolayers has been reported in a number of experimental as well as theoretical works (see e.g. [18–20]).

Individual monolayers of TMDs are usually ferromagnetic with the magnetization oriented in the layer plane, though systems with magnetization normal to the plane can also occur. Moreover, antiferromagnetically arranged monolayers are possible as well. Of particular interest seem to be the bilayer structures, especially those with ferromagnetic monolayers coupled antiferromagnetically due to interlayer exchange coupling. This is because such bilayers in an external magnetic field may be considered as natural atomically thin spin valves [4], and may be a fundamental building blocks of two dimensional spintronics.

In this paper we analyse spin wave excitations in the H-stacked as well as T-stacked bilayers of TMDs, with particular attention to the interplay of the magnetocrystalline anisotropy, intralayer ferromagnetic exchange coupling, and interlayer antiferromagnetic or ferromagnetic coupling. In order to find the magnon spectra we use the relevant spin Hamiltonian and apply the Holstein-Primakoff transformation followed by the diagonalization procedure based on the Bogolubov transformation [22, 32–34].

Vanadium-based dichalcogenides usually display an easy-plane single-ion magnetic anisotropy – though easy-axis single-ion anisotropy normal to the plane has also been found owing to the proximity effects [35]. Such an anisotropy has been proven by many DFT numerical calculations and also evaluated experimentally, so its presence in TMDs is now well established [19, 20, 35–39] – even though a single-ion magnetic anisotropy for spin 1/2 model was believed to vanish. Moreover, it was shown that this magnetic anisotropy can be tuned externally, eg. by a strain [40].

In turn, the existence of an in-plane easy-axis anisotropy is not so clear. Such an anisotropy was found in Ref. [19], however it was about two orders of magnitude smaller than the corresponding easy-plane anisotropy. On one hand, existence of such an in-plane easy-axis single-ion anisotropy is believed to vanish for spin 1/2 models, and also on symmetry arguments. However, there are several ingredients that may effectively contribute to such an anisotropy. First of all, exact value of the magnetic moments of V atoms in V-based TMDs deviates from $1\mu_B$, as follows from DFT calculations and also from experimental measurements, indicating that these materials cannot not be described by strictly spin 1/2 models. Secondly, some other contributions may be due to magnetic dipolar interactions, spin-orbit interaction associated with mobile electrons, proximity to a sub-

strate, and external strains. Especially the latter seems to be very effective and important.

Therefore, in our paper we assume the easy-plane anisotropy, and following Ref. [19], we also assume a small in-plane easy-axis anisotropy (two orders of magnitude smaller than the easy-plane anisotropy, as in Ref. [19]). Though the later anisotropy is rather difficult to be detected experimentally, especially in the spin-wave spectrum, we include it to have a general situation and general formulas that can be used if necessary for materials where such an anisotropy is larger, especially that this anisotropy is also tunable externally. Therefore, one may expect that some data on higher values of the easy-axis anisotropy will be available in the near future, e.g. in strained systems. However, for numerical calculations of spinwave modes we assume the value given in Ref. [19], and the role of easy-plane and in-plane easy-axis anisotropies is analyzed in detail.

The model and theoretical method used to study spin wave spectra are described in more details in section 2, where the spin Hamiltonian used to describe TMDs is defined. Numerical results are presented and discussed in section 3. Summary and final conclusions are in section 4.

II. ANTIFERROMAGNETICALLY COUPLED BILAYERS

We consider the case when the perpendicular anisotropy is of easy-plane type, and assume the coordinate system with the axis y normal to the layers and the axis z along the in-plane easy axis. Though the in-plane easy-axis anisotropy is rather small in Vanadium dichalcogenides, we consider a general model when this anisotropy may be remarkable and may play some role. We also assume an external magnetic field along the easy axis.

To describe spin waves in a bilayer consisting of two ferromagnetic monolayers coupled antiferromagnetically we use the following model spin Hamiltonian:

$$H = \sum_{\alpha} H^{\alpha} + H_{\text{int}}, \quad (1)$$

where $\alpha=T$ ($\alpha=B$) stands the top (bottom) monolayer, and Hamiltonian of the α th monolayer includes three terms, $H^{\alpha} = H_{\text{ex}}^{\alpha} + H_A^{\alpha} + H_h^{\alpha}$. Here, the first term stands for the ferromagnetic intralayer exchange coupling, the second term includes the magnetic anisotropies in the system, and the last term is the Zeemann energy in an external magnetic field h . The Hamiltonian H^{α} can be written explicitly in the form,

$$H^{\alpha} = J_1 \sum_{\mathbf{r}, \delta} \mathbf{S}_{\mathbf{r}, \alpha} \cdot \mathbf{S}_{\mathbf{r} + \delta, \alpha} + \frac{D_y}{2} \sum_{\mathbf{r}} \left(S_{\mathbf{r}, \alpha}^y \right)^2 - \frac{D_z}{2} \sum_{\mathbf{r}} \left(S_{\mathbf{r}, \alpha}^z \right)^2 - h \sum_{\mathbf{r}} S_{\mathbf{r}, \alpha}^z. \quad (2)$$

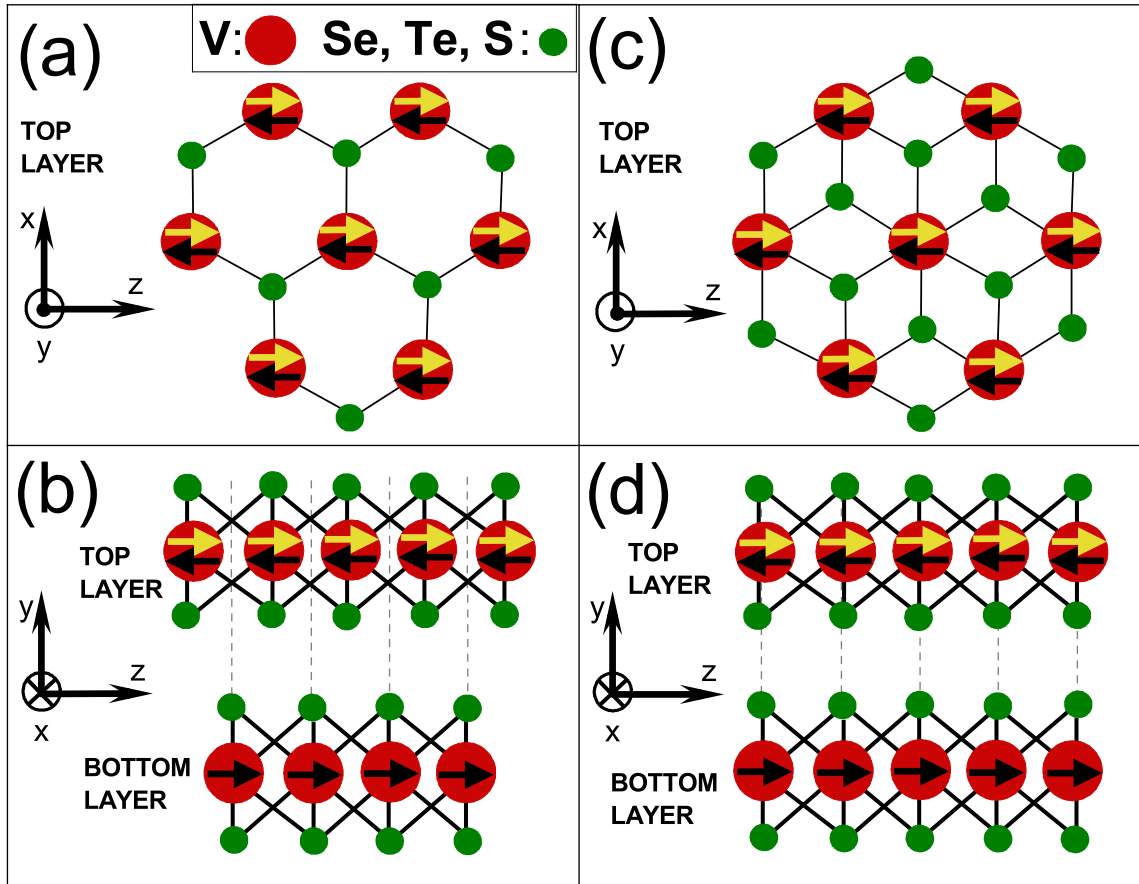


FIG. 1. Top view of the VX_2 ($X= \text{Se}, \text{Te}, \text{S}$) monolayer in the H-phase (a) and T-phase (c). The monolayer is in the (x, z) plane while the axis y is normal to the plane. The side view of the corresponding bilayer systems along the z -axis is shown in (b) and (c) for the H and T phases, respectively. Ground state spin orientation of the bottom layer is assumed along the z -axis while that of the top layer is along $-z$ axis for the antiferromagnetically coupled bilayers (black arrows) and along z axis for the ferromagnetic bilayers (yellow arrows). For the trigonal prismatic structure (H-phase), one monolayer sits on the other with π rotation, which implies that each vanadium atom (see the position of the red dots) has three NNs in the adjacent monlayer. For the octahedral structure (T-phase) of VX_2 , each vanadium atom has one NN in the adjacent monlayer.

Here, the exchange coupling between Vanadium atoms within the monolayer is ferromagnetic, $J_1 < 0$, the easy-plane anisotropy constant D_y and the in-plane easy-axis anisotropy constant D_z are both defined as positive, while the magnetic field h is taken in energy units ($g\mu_B h \Rightarrow h$, where g denotes the gyromagnetic factor and μ_B is the Bohr magneton). The summation over \mathbf{r} denotes here the summation over lattice sites, while that over δ is the summation over nearest neighbours, with δ standing for the vectors connecting a particular site to its in-plane nearest neighbours (NNs). [We neglect here exchange coupling between next-nearest neighbours.] In turn, the last term in Eq.(1) describes the antiferromag-

netic exchange coupling between the two monolayers,

$$H_{int} = 2J_2 \sum_{\mathbf{r}, \delta} \mathbf{S}_{\mathbf{r}, T} \cdot \mathbf{S}_{\mathbf{r}+\delta, B}, \quad (3)$$

with $J_2 > 0$. Here, the summation is over lattice sites \mathbf{r} in one monolayer only (therefore, there is a factor of 2 in front on the right side). Note, δ corresponds here to inter-layer NNs (NNs in the adjacent layer).

When the above defined system is in an external magnetic field applied along the in-plane easy axis (z axis), one may expect in general three different stable spin configurations in the bilayer; (i) antiferromagnetic state with

the spins of the bottom layer oriented say along $+z$ axis and of the top layer along $-z$ axis, respectively, (ii) spin-flop (canted) phase with the spins of the two monolayers oriented in the atomic planes at an angle χ to the z axis, and (iii) the ferromagnetic phase with the spins of both layers oriented along the z axis (this corresponds to $\chi = 0$). The transition from antiferromagnetic to spin-flop phase occurs at $h = h_{\text{sf}}$ (see Appendix A), with

$$h_{\text{sf}} = S\sqrt{D_z(4\xi J_2 - D_z)} \quad (4)$$

for $4\xi J_2 - D_z > 0$, where ξ denotes the structure factor, $\xi = 3$ and $\xi = 1$ for the H and T phases, respectively. The spin-flop phase appears in the range of magnetic fields $h_{\text{sf}} < h < h_s$, where h_s is the threshold magnetic field (the saturation field), at which the transition from the spin-flop phase to the ferromagnetic one occurs (see Appendix A),

$$h_s = S(4\xi J_2 - D_z). \quad (5)$$

If $D_z = 0$, then $h_{\text{sf}} = 0$ and $h_s = 4S\xi J_2$. Note, that in a general case the spin-flop phase appears when $4\xi J_2 > D_z$, while in the opposite case, $4\xi J_2 < D_z$, there is a direct (metamagnetic) transition from the antiferromagnetic to ferromagnetic phase (there is then no spin-flop phase). In the systems considered here D_z is very small, much smaller than J_2 . Accordingly, the spin-flop field h_{sf} is also very small, so there is no metamagnetic transition and the antiparallel configuration may occur in a very narrow range of magnetic field and also at very low temperatures.

A. Spin waves in the antiferromagnetic phase

We consider first the antiferromagnetic (AF) phase, which appears below the transition field to the spin-flop phase. The spin moments of the bottom layer are along z axis, while of the top layer are along the $-z$ axis, see Fig.1. In the first step we perform the Holstein-Primakoff transformation:

$$\begin{aligned} S_{\mathbf{r},T}^x &= \sqrt{\frac{S}{2}}(a_{\mathbf{r},T}^+ + a_{\mathbf{r},T}), \\ S_{\mathbf{r},T}^y &= i\sqrt{\frac{S}{2}}(a_{\mathbf{r},T} - a_{\mathbf{r},T}^+), \\ S_{\mathbf{r},T}^z &= a_{\mathbf{r},T}^+ a_{\mathbf{r},T} - S, \end{aligned} \quad (6)$$

for spins oriented antiparallel to the z -axis (top layer), and

$$\begin{aligned} S_{\mathbf{r},B}^x &= \sqrt{\frac{S}{2}}(a_{\mathbf{r},B}^+ + a_{\mathbf{r},B}), \\ S_{\mathbf{r},B}^y &= i\sqrt{\frac{S}{2}}(a_{\mathbf{r},B}^+ - a_{\mathbf{r},B}), \\ S_{\mathbf{r},B}^z &= S - a_{\mathbf{r},B}^+ a_{\mathbf{r},B}, \end{aligned} \quad (7)$$

for spins oriented along the z -axis (bottom layer). Here, $a_{\mathbf{r},\alpha}^+$ ($a_{\mathbf{r},\alpha}$) is the bosonic creation (annihilation) operator.

Upon inserting the Holstein-Primakoff transformation into Eqs. (1) to (3), keeping terms up to the second order in the magnon operators and disregarding any constant terms, one finds,

$$\begin{aligned} H &= J_1 S \sum_{\mathbf{r},\delta,\alpha} \left(a_{\mathbf{r},\alpha}^+ a_{\mathbf{r},\alpha} + a_{\mathbf{r}+\delta,\alpha}^+ a_{\mathbf{r}+\delta,\alpha} \right. \\ &\quad \left. - a_{\mathbf{r},\alpha}^+ a_{\mathbf{r}+\delta,\alpha} - a_{\mathbf{r}+\delta,\alpha}^+ a_{\mathbf{r},\alpha} \right) + 2J_2 S \sum_{\mathbf{r}} \left[\sum_{\alpha} a_{\mathbf{r},\alpha}^+ a_{\mathbf{r},\alpha} \right. \\ &\quad \left. + \sum_{\delta} \left(a_{\mathbf{r},T}^+ a_{\mathbf{r}+\delta,B}^+ + a_{\mathbf{r},T} a_{\mathbf{r}+\delta,B} \right) \right] \\ &\quad - \frac{D_y S}{4} \sum_{\mathbf{r},\alpha} \left(a_{\mathbf{r},\alpha}^+ a_{\mathbf{r},\alpha}^+ + a_{\mathbf{r},\alpha} a_{\mathbf{r},\alpha} - 2a_{\mathbf{r},\alpha}^+ a_{\mathbf{r},\alpha} \right) \\ &\quad + D_z S \sum_{\mathbf{r},\alpha} a_{\mathbf{r},\alpha}^+ a_{\mathbf{r},\alpha} - h \sum_{\mathbf{r}} \left(a_{\mathbf{r},B}^+ a_{\mathbf{r},B} - a_{\mathbf{r},T}^+ a_{\mathbf{r},T} \right). \end{aligned} \quad (8)$$

Then we perform the Fourier transformation to the momentum space,

$$\begin{aligned} a_{\mathbf{r},\alpha} &= \frac{1}{\sqrt{N}} \sum_{\mathbf{k}} a_{\mathbf{k},\alpha} e^{-i\mathbf{k}\cdot\mathbf{r}}, \\ a_{\mathbf{r},\alpha}^+ &= \frac{1}{\sqrt{N}} \sum_{\mathbf{k}} a_{\mathbf{k},\alpha}^+ e^{i\mathbf{k}\cdot\mathbf{r}}, \end{aligned} \quad (9)$$

where N is the number of unit cells, and \mathbf{k} is the wavevector from the first Brillouin zone, see Appendix B. Upon this transformation one may rewrite Hamiltonian, Eq. (8), in the following form:

$$\begin{aligned} H &= \sum_{\mathbf{k}} \left\{ 2J_1 S \sum_{\alpha} (\gamma_{\mathbf{k}} - 6) a_{\mathbf{k},\alpha}^+ a_{\mathbf{k},\alpha} \right. \\ &\quad \left. + 2J_2 S \left(\sum_{\alpha} \xi a_{\mathbf{k},\alpha}^+ a_{\mathbf{k},\alpha} + \eta_{\mathbf{k}} a_{-\mathbf{k},T}^+ a_{\mathbf{k},B}^+ + \eta_{\mathbf{k}}^* a_{-\mathbf{k},T} a_{\mathbf{k},B} \right) \right. \\ &\quad \left. + S \sum_{\alpha} \left[-\frac{D_y}{4} (a_{\mathbf{k},\alpha}^+ a_{-\mathbf{k},\alpha}^+ + a_{\mathbf{k},\alpha} a_{-\mathbf{k},\alpha} - 2a_{\mathbf{k},\alpha}^+ a_{\mathbf{k},\alpha}) \right. \right. \\ &\quad \left. \left. + D_z a_{\mathbf{k},\alpha}^+ a_{\mathbf{k},\alpha} \right] + h (a_{\mathbf{k},B}^+ a_{\mathbf{k},B} - a_{\mathbf{k},T}^+ a_{\mathbf{k},T}) \right\}, \end{aligned} \quad (10)$$

where the quantity ξ is defined below Eq. (4), while the structure factors $\gamma_{\mathbf{k}}$ and $\eta_{\mathbf{k}}$ read

$$\gamma_{\mathbf{k}} = 2 \left(\cos(k_z a) + 2 \cos\left(\frac{\sqrt{3}}{2} k_x a\right) \cos\left(\frac{1}{2} k_z a\right) \right), \quad (11)$$

$$\eta_{\mathbf{k}} = \begin{cases} 1 & \text{(for T phase)} \\ e^{i\frac{k_x a}{\sqrt{3}}} + 2e^{-i\frac{k_x a}{2\sqrt{3}}} \cos\left(\frac{1}{2} k_z a\right) & \text{(for H phase)}. \end{cases} \quad (12)$$

As one can easily note, Eq.(10) may be written as

$$H = H_{\mathbf{k}} + H_{-\mathbf{k}}, \quad (13)$$

where

$$H_{\mathbf{k}} = \sum_{\mathbf{k}} \left[\left(\frac{A_{\mathbf{k}}^+}{2} \right) a_{\mathbf{k},B}^+ a_{\mathbf{k},B} + \left(\frac{A_{\mathbf{k}}^-}{2} \right) a_{\mathbf{k},T}^+ a_{\mathbf{k},T} \right. \\ \left. + B_{\mathbf{k}} a_{-\mathbf{k},T} a_{\mathbf{k},B} + C \sum_{\alpha} a_{\mathbf{k},\alpha} a_{-\mathbf{k},\alpha} \right] + H.c., \quad (14)$$

with the coefficients $A_{\mathbf{k}}^{\pm}$, $B_{\mathbf{k}}$ and C given by the formulae,

$$A_{\mathbf{k}}^{\pm} = S \left[2J_1(\gamma_{\mathbf{k}} - 6) + 2\xi J_2 + \frac{D_y}{2} + D_z \right] \pm h, \\ B_{\mathbf{k}} = 2\eta_{\mathbf{k}}^* J_2 S, \\ C = -\frac{D_y S}{4}. \quad (15)$$

Following Refs [22, 32–34], we define now a new wave vector $\boldsymbol{\kappa}$ that runs over half of the vector space of \mathbf{k} , and define the four-dimensional Bogolubov transformation to new bosonic operators $\Theta_{\pm\boldsymbol{\kappa},\mu}$ and $\Theta_{\pm\boldsymbol{\kappa},\mu}^+$, with $\mu = +, -$ indexing the two magnon modes (to be specified below). This transformation can be written as

$$\Theta_{\boldsymbol{\kappa}} = \hat{T}_4 \mathbf{a}_{\mathbf{k}}, \quad (16)$$

where

$$\Theta_{\boldsymbol{\kappa}} = \begin{pmatrix} \Theta_{\boldsymbol{\kappa},I} \\ \Theta_{\boldsymbol{\kappa},II} \\ \Theta_{-\boldsymbol{\kappa},I}^+ \\ \Theta_{-\boldsymbol{\kappa},II}^+ \end{pmatrix}, \quad \mathbf{a}_{\mathbf{k}} = \begin{pmatrix} a_{\mathbf{k},T} \\ a_{\mathbf{k},B} \\ a_{-\mathbf{k},T}^+ \\ a_{-\mathbf{k},B}^+ \end{pmatrix}, \quad (17)$$

and \hat{T}_4 denotes a $2\mathcal{N} \times 2\mathcal{N}$ paraunitary matrix (\mathcal{N} is a number of internal degrees of freedom within the unit cell), which obeys

$$[\Theta_{\boldsymbol{\kappa}}, \Theta_{\boldsymbol{\kappa}}^+] = \hat{T}_4 [a_{\mathbf{k}}, a_{\mathbf{k}}^+] \hat{T}_4^+ = \hat{T}_4 \hat{\sigma}_z \hat{T}_4^+ = \hat{\sigma}_z, \quad (18)$$

with the diagonal matrix $(\hat{\sigma}_z)_{l,l'} = \delta_{l,l'} \sigma_l$, where $\sigma_l = 1$ for $l \leq \mathcal{N}$ and $\sigma_l = -1$ otherwise. The requirement given by Eq. (18) follows from the bosonic commutation relations $[\Theta_{\boldsymbol{\kappa},\mu}, \Theta_{\boldsymbol{\kappa}',\mu'}^+] = \delta_{\boldsymbol{\kappa},\boldsymbol{\kappa}'} \delta_{\mu,\mu'}$. As a consequence, Eq. (16) can be written in the form

$$\Theta_{\boldsymbol{\kappa}} = \sum_{\alpha} \begin{pmatrix} u_{I,\alpha} & v_{I,\alpha} \\ u_{II,\alpha} & v_{II,\alpha} \\ \tilde{u}_{I,\alpha} & \tilde{v}_{I,\alpha} \\ \tilde{u}_{II,\alpha} & \tilde{v}_{II,\alpha} \end{pmatrix} \begin{pmatrix} a_{\mathbf{k},\alpha} \\ a_{-\mathbf{k},\alpha}^+ \end{pmatrix}, \quad (19)$$

where the Bogolubov coefficients $u_{\mu,\alpha}$ and $v_{\mu,\alpha}$ are evaluated at $\boldsymbol{\kappa}$ while the coefficients $\tilde{u}_{\mu,\alpha}$ and $\tilde{v}_{\mu,\alpha}$ are evaluated at $-\boldsymbol{\kappa}$. Moreover, the relation (19) requires the normalization

$$\sum_{\alpha} (|u_{\mu,\alpha}|^2 + |v_{\mu,\alpha}|^2) = 1, \quad \sum_{\alpha} (|\tilde{u}_{\mu,\alpha}|^2 + |\tilde{v}_{\mu,\alpha}|^2) = 1. \quad (20)$$

This procedure finally diagonalizes the Hamiltonian,

$$H = \sum_{\boldsymbol{\kappa},\mu} \left(\omega_{\boldsymbol{\kappa},\mu} \Theta_{\boldsymbol{\kappa},\mu}^+ \Theta_{\boldsymbol{\kappa},\mu} + \omega_{-\boldsymbol{\kappa},\mu} \Theta_{-\boldsymbol{\kappa},\mu}^+ \Theta_{-\boldsymbol{\kappa},\mu} \right). \quad (21)$$

Employing Eq. (21), one obtains the relation $[\Theta_{\boldsymbol{\kappa},\mu}, H] = \omega_{\boldsymbol{\kappa},\mu} \Theta_{\boldsymbol{\kappa},\mu}$, from which Eqs. (14) and (19) lead to the eigenvalue problem

$$\Lambda_{\boldsymbol{\kappa}} \mathbf{e}_{\mu} = \omega_{\boldsymbol{\kappa},\mu} \mathbf{e}_{\mu}, \quad (22)$$

with

$$\Lambda_{\boldsymbol{\kappa}} = \begin{pmatrix} A_{\boldsymbol{\kappa}}^- & 0 & -2C & -B_{\boldsymbol{\kappa}}^* \\ 0 & A_{\boldsymbol{\kappa}}^+ & -B_{\boldsymbol{\kappa}} & -2C \\ 2C & B_{\boldsymbol{\kappa}}^* & -A_{\boldsymbol{\kappa}}^- & 0 \\ B_{\boldsymbol{\kappa}} & 2C & 0 & -A_{\boldsymbol{\kappa}}^+ \end{pmatrix}, \quad \mathbf{e}_{\mu} = \begin{pmatrix} u_{\mu,T} \\ u_{\mu,B} \\ v_{\mu,T} \\ v_{\mu,B} \end{pmatrix}. \quad (23)$$

Note that $A_{\boldsymbol{\kappa}}^{\pm} = A_{-\boldsymbol{\kappa}}^{\pm}$, $B_{\boldsymbol{\kappa}}^* = B_{-\boldsymbol{\kappa}}$ and therefore we have $u_{\mu,\alpha} = \tilde{u}_{\mu,\alpha}$, $v_{\mu,\alpha} = \tilde{v}_{\mu,\alpha}$. Moreover, as $\omega_{\boldsymbol{\kappa},\mu}$ is a real quantity, we also have $\omega_{-\boldsymbol{\kappa},\mu} = \omega_{\boldsymbol{\kappa},\mu}$. Finally, from Eqs. (22) and (23) one finds the appropriate dispersion relation.

For convenience, in this dispersion relation we come back to the usual notation for the wavevector, and replace in this relation $\boldsymbol{\kappa}$ by \mathbf{k} , which makes no confusion and no ambiguity. Thus, we write the dispersion relation as

$$\omega_{\mathbf{k},\mu} = \left\{ A_{\mathbf{k}}^2 - |B_{\mathbf{k}}|^2 - 4C^2 + h^2 \right. \\ \left. \pm 2 \left[4C^2 |B_{\mathbf{k}}|^2 + h^2 (A_{\mathbf{k}}^2 - |B_{\mathbf{k}}|^2) \right]^{\frac{1}{2}} \right\}^{\frac{1}{2}}, \quad (24)$$

where $A_{\mathbf{k}} \equiv A_{\mathbf{k}}^{\pm} \mp h$, and the sign $+$ and $-$ in the fifth term on the right hand side of Eq. (24) corresponds to the spin-wave mode index $\mu = +$ and $\mu = -$, respectively. From this equation follows that nonzero easy-plane anisotropy, $D_y > 0$, leads to splitting of the magnon spectrum in the absence of magnetic field, $h = 0$, into two branches, $\omega_{\mathbf{k},\pm}$.

In the center of the first Brillouin zone, $\mathbf{k} = \mathbf{0}$ (point Γ), one then finds

$$\omega_{\mathbf{k}=0,\pm} = S [2\xi J_2 (D_y \pm D_y + 2D_z) + D_y D_z + D_z^2]^{\frac{1}{2}}. \quad (25)$$

This formula clearly shows that splitting of the magnon modes at the Γ point appears for a nonzero D_y . In turn, a nonzero in-plane magnetic anisotropy, $D_z > 0$, leads to an energy gap. If $D_y = 0$ and $D_z > 0$, then the energy gap at Γ is given by

$$\omega_{\mathbf{k}=0,+} = \omega_{\mathbf{k}=0,-} = S (4\xi J_2 D_z + D_z^2)^{\frac{1}{2}}. \quad (26)$$

This gap vanishes if $D_z = 0$, i.e., a two-fold degenerated Goldstone mode, $\omega_{\mathbf{k}=0,\pm} = 0$, then appears. If $D_z = 0$ and $D_y > 0$, then

$$\omega_{\mathbf{k}=0,+} = S (4\xi J_2 D_y)^{\frac{1}{2}}, \quad (27)$$

$$\omega_{\mathbf{k}=0,-} = 0 \quad (\text{Goldstone mode}). \quad (28)$$

B. Spin waves in the spin-flop phase

In the spin-flop phase, $h_{\text{sf}} < h < h_s$, one needs first to rotate the spin operators to the local quantization axes appropriate for the top (T) and bottom (B) layers (see Appendix A). This transformation does not affect the ferromagnetic intralayer exchange term of the model Hamiltonian (1,2), while the antiferromagnetic interlayer coupling term H_{int} as well as the anisotropy H_A^α and Zeeman H_h^α terms now become

$$H_{\text{int}} = 2J_2 \sum_{\mathbf{r}, \delta} [\cos 2\chi (S_{\mathbf{r},T}^z S_{\mathbf{r}+\delta,B}^z - S_{\mathbf{r},T}^x S_{\mathbf{r}+\delta,B}^x) - S_{\mathbf{r},T}^y S_{\mathbf{r}+\delta,B}^y], \quad (29)$$

$$H_A^\alpha = \frac{1}{2} \sum_{\mathbf{r}} \left\{ D_y (S_{\mathbf{r},\alpha}^y)^2 - D_z [(S_{\mathbf{r},\alpha}^x)^2 \sin^2 \chi + (S_{\mathbf{r},\alpha}^z)^2 \cos^2 \chi] \right\}, \quad (30)$$

$$H_h^\alpha = -h \cos \chi \sum_{\mathbf{r}} S_{\mathbf{r},\alpha}^z, \quad (31)$$

where the spin operators are in the corresponding local systems.

Upon Holstein-Primakoff and Fourier transformations (see Appendix C), one arrives at the Hamiltonian, which – bearing in mind the Bogolubov transformation – can be written as $H = H_{\mathbf{k}} + H_{-\mathbf{k}}$, where

$$H_{\mathbf{k}} = \sum_{\mathbf{k}} \left[\sum_{\alpha} \left(\frac{A_{\mathbf{k}}}{2} \right) a_{\mathbf{k},\alpha}^+ a_{\mathbf{k},\alpha} + B_{\mathbf{k}} a_{-\mathbf{k},T} a_{\mathbf{k},B} + \tilde{B}_{\mathbf{k}} a_{\mathbf{k},T}^+ a_{\mathbf{k},B} + C \sum_{\alpha} a_{\mathbf{k},\alpha} a_{-\mathbf{k},\alpha} \right] + H.c., \quad (32)$$

with

$$\begin{aligned} A_{\mathbf{k}} &= S \left[2J_1 (\gamma_{\mathbf{k}} - 6) - 2\xi J_2 \cos 2\chi + \frac{D_y}{2} + \frac{D_z}{2} (3 \cos^2 \chi - 1) \right] + h \cos \chi, \\ B_{\mathbf{k}} &= 2\eta_{\mathbf{k}}^* J_2 S \sin^2 \chi, \\ \tilde{B}_{\mathbf{k}} &= -2\eta_{\mathbf{k}}^* J_2 S \cos^2 \chi, \\ C &= -\frac{S}{4} (D_y + D_z \sin^2 \chi). \end{aligned} \quad (33)$$

Then, the diagonalization of the Eq. (32), similarly as described in the preceding subsection, leads to the eigenvalue problem, $\Lambda_{\kappa} \mathbf{e}_{\mu} = \omega_{\kappa,\mu} \mathbf{e}_{\mu}$, where

$$\Lambda_{\kappa} = \begin{pmatrix} A_{\kappa} & \tilde{B}_{\kappa} & -2C & -B_{\kappa}^* \\ \tilde{B}_{\kappa} & A_{\kappa} & -B_{\kappa} & -2C \\ 2C & B_{\kappa}^* & -A_{\kappa} & -\tilde{B}_{\kappa}^* \\ B_{\kappa} & 2C & -\tilde{B}_{\kappa} & -A_{\kappa} \end{pmatrix}, \mathbf{e}_{\mu} = \begin{pmatrix} u_{\mu,T} \\ u_{\mu,B} \\ v_{\mu,T} \\ v_{\mu,B} \end{pmatrix}. \quad (34)$$

Upon replacing the notation κ by \mathbf{k} , we write the dispersion relation in the form

$$\begin{aligned} \omega_{\mathbf{k},\mu} &= \left\{ A_{\mathbf{k}}^2 - |B_{\mathbf{k}}|^2 + |\tilde{B}_{\mathbf{k}}|^2 - 4C^2 \right. \\ &\quad \pm \left[-8A_{\mathbf{k}} C (B_{\mathbf{k}}^* \tilde{B}_{\mathbf{k}} + B_{\mathbf{k}} \tilde{B}_{\mathbf{k}}^*) + B_{\mathbf{k}}^2 \tilde{B}_{\mathbf{k}}^{*2} \right. \\ &\quad \left. \left. + B_{\mathbf{k}}^{*2} \tilde{B}_{\mathbf{k}}^2 + 16|B_{\mathbf{k}}|^2 C^2 + 4A_{\mathbf{k}}^2 |\tilde{B}_{\mathbf{k}}|^2 - 2|B_{\mathbf{k}}|^2 |\tilde{B}_{\mathbf{k}}|^2 \right]^{\frac{1}{2}} \right\}^{\frac{1}{2}}, \end{aligned} \quad (35)$$

with the + and – signs in the fifth term on the right hand side of Eq. (35) corresponding to the mode index $\mu = +$ and $\mu = -$, respectively. It is worth noting here that in case of the T-stacked geometry, both $B_{\mathbf{k}}$ and $\tilde{B}_{\mathbf{k}}$ are independent of \mathbf{k} , $B_{\mathbf{k}} = B$, $\tilde{B}_{\mathbf{k}} = \tilde{B}$, so that Eq. (35) simplifies to the following one:

$$\omega_{\mathbf{k},\mu} = \left\{ (A_{\mathbf{k}} - \tilde{B})^2 - (B \pm 2C)^2 \right\}^{\frac{1}{2}}. \quad (36)$$

At the saturation field h_s and for $\mathbf{k} = \mathbf{0}$, the magnon energies are equal

$$\omega_{\mathbf{k}=0,\mu} = S \left[\left(2\xi J_2 \pm 2\xi J_2 + \frac{D_y}{2} \right)^2 - \left(\frac{D_y}{2} \right)^2 \right]^{\frac{1}{2}}. \quad (37)$$

Thus, one finds

$$\omega_{\mathbf{k}=0,+} = 2S \left[(2\xi J_2)^2 + 2\xi J_2 \frac{D_y}{2} \right]^{\frac{1}{2}}, \quad (38)$$

$$\omega_{\mathbf{k}=0,-} = 0 \quad (\text{Goldstone mode}). \quad (39)$$

Thus, at the saturation field h_s , one of the modes is the Goldstone mode – even in the case of nonzero in-plane easy-axis anisotropy, while the splitting of the modes (gap between the two modes) appears also in the case of vanishing D_y . This behaviour is different from that in the antiferromagnetic state.

C. Ferromagnetic state above the saturation field

For $h \geq h_s$, the system is in the saturated (ferromagnetic) state, which can be considered as a special case of the spin-flop phase, corresponding to $\chi = 0$. Equations (29) to (31) take then the forms

$$H_{\text{int}} = 2J_2 \sum_{\mathbf{r}, \delta} (S_{\mathbf{r},T}^z S_{\mathbf{r}+\delta,B}^z - S_{\mathbf{r},T}^x S_{\mathbf{r}+\delta,B}^x - S_{\mathbf{r},T}^y S_{\mathbf{r}+\delta,B}^y), \quad (40)$$

$$H_A^\alpha = \frac{1}{2} \sum_{\mathbf{r}} \left[D_y (S_{\mathbf{r},\alpha}^y)^2 - D_z (S_{\mathbf{r},\alpha}^z)^2 \right], \quad (41)$$

$$H_h^\alpha = -h \sum_{\mathbf{r}} S_{\mathbf{r},\alpha}^z. \quad (42)$$

Accordingly, the system Hamiltonian upon Holstein-Primakoff and Fourier transformations acquires the form (32) with $A_{\mathbf{k}}$, $B_{\mathbf{k}}$, $\tilde{B}_{\mathbf{k}}$ and C given by the formulas

$$\begin{aligned} A_{\mathbf{k}} &= S \left[2J_1(\gamma_{\mathbf{k}} - 6) - 2\xi J_2 + \frac{D_y}{2} + D_z \right] + h, \\ B_{\mathbf{k}} &= 0, \\ \tilde{B}_{\mathbf{k}} &= -2\eta_{\mathbf{k}}^* J_2 S, \\ C &= -\frac{SD_y}{4}. \end{aligned} \quad (43)$$

Thus, the eigenvalue problem, $\Lambda_{\kappa} e_{\mu} = \omega_{\kappa, \mu} e_{\mu}$, with

$$\Lambda_{\kappa} = \begin{pmatrix} A_{\kappa} & \tilde{B}_{\kappa}^* & -2C & 0 \\ \tilde{B}_{\kappa} & A_{\kappa} & 0 & -2C \\ 2C & 0 & -A_{\kappa} & -\tilde{B}_{\kappa}^* \\ 0 & 2C & -\tilde{B}_{\kappa} & -A_{\kappa} \end{pmatrix}, e_{\mu} = \begin{pmatrix} u_{\mu, T} \\ u_{\mu, B} \\ v_{\mu, T} \\ v_{\mu, B} \end{pmatrix}, \quad (44)$$

leads to the final dispersion relation for the ferromagnetic phase in the form

$$\omega_{\kappa, \mu} = \left[(A_{\kappa} \pm \tilde{B}_{\kappa})^2 - 4C^2 \right]^{\frac{1}{2}}. \quad (45)$$

III. NUMERICAL RESULTS AND DISCUSSION

To discuss properties of spin-wave spectra in 2H-VX₂ bilayer systems, we need first to fix the appropriate parameters, including the exchange and magnetic anisotropy constants, as well as the appropriate structural parameters. As an example we will consider the spinwave spectra of a VTe₂ bilayer, and take the relevant parameters from DFT calculations [41]. Accordingly we assume: lattice parameter $a = 3.59\text{\AA}$, $D_y = 3.812$ meV, $J_1 = -14.85$ meV, and $J_2 = 0.19$ meV. Since the model description is based on spin-1/2 Hamiltonian ($S = 1/2$), the DFT-calculated exchange parameters have been adapted accordingly. Only the in-plane easy-axis anisotropy constant, $D_z = 0.016$ meV, was taken from Ref.[19]. According to Eqs. (4) and (5), the corresponding threshold magnetic fields h_{sf} and h_s (converted from energy units to Tesla) are $h_{\text{sf}} = 0.82$ T and $h_s = 9.65$ T.

The three-dimensional (3D) presentation of the magnon spectrum, calculated for the 2H-VTe₂ bilayer in the antiferromagnetic phase and in the absence of external magnetic field (antiparalle configuration) is shown in Fig.2a. As there are two magnetic atoms in the unit cell of the considered bilayer, one can expect two magnon bands. In the absence of magnetic field, $h = 0$, these two magnon modes have similar energy so they are not resolved in Fig.2a. However, even for $h = 0$, these two modes can differ slightly in energy due to other interactions, like interlayer exchange coupling and the easy-plane and in-plane easy-axis magnetic anisotropies. These interactions introduce subtle effects (not resolved within the energy scale of Fig. 2a), which may lead to

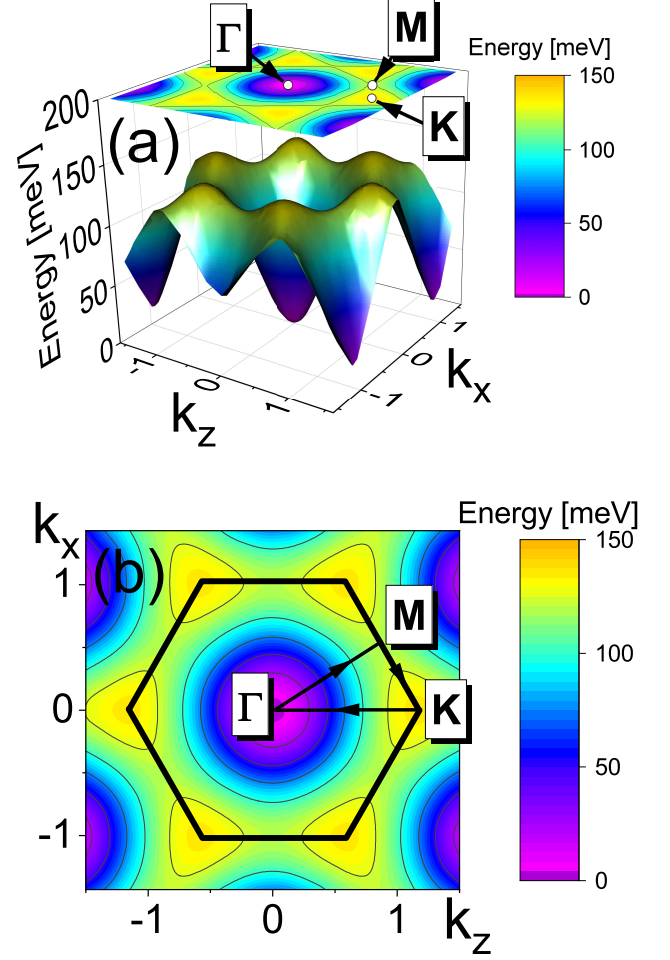


FIG. 2. The 3D view of the magnon band in the first Brillouin zone, in the absence magnetic field ($h = 0$), calculated for the 2H-VTe₂ bilayer (a) and its projection onto the (k_z, k_x) -plane (b) with indicated Brillouin zone center (Γ) and high-symmetry points (K,M) and paths. See text for more details.

a splitting of the spectrum into two spin-wave modes at zero external magnetic field, and also can generate a gap in the spectrum, as will be shown below. Low energy spin waves exist in the Brillouin zone center around $\mathbf{k} = \mathbf{0}$ (see the Γ point in Fig. 2a), while the maxima of magnon energy appear at the points K of the Brillouin zone (see Fig. 2a,b). The spin-wave energy for selected cross sections of the 3D magnon bands are displayed Fig.2b and Fig.3a along high-symmetry paths, $K \rightarrow \Gamma \rightarrow M \rightarrow K$, in the momentum space.

Explicit dispersion relations along the $\Gamma \rightarrow K$ and $\Gamma \rightarrow M \rightarrow K$ paths in the Brillouin zone are shown in Fig.3a. Though there are two modes in the bilayers under considerations, separation of these two modes is not resolved in Fig.3a. Therefore, in Fig.3b we zoomed in a small area near the Γ point. Now, splitting of the modes is clearly seen. Moreover, this figure also shows that there is a gap in the spectrum at the Γ point, i.e.

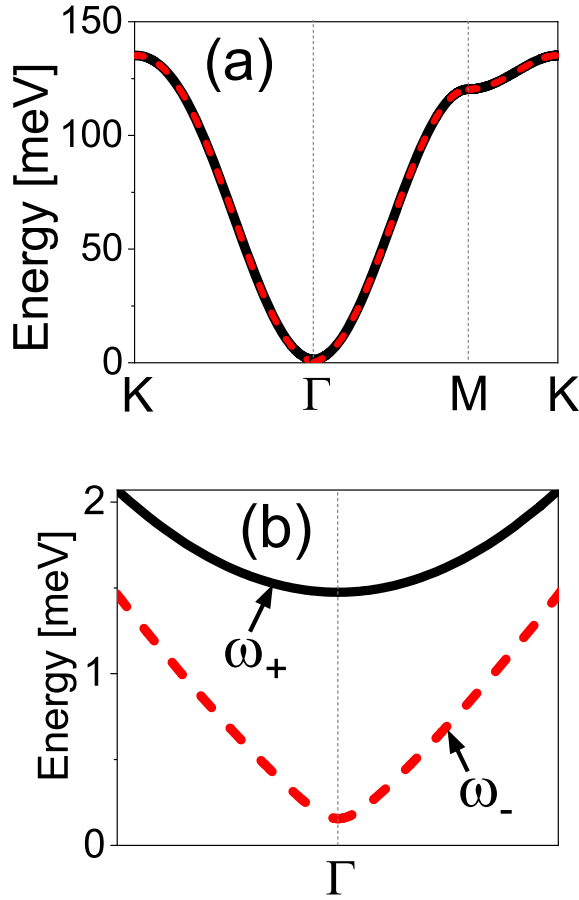


FIG. 3. Dispersion curves of the spin wave spectrum along the path K- Γ -M-K (a). As in Fig.2, the two modes are not resolved here. To observe splitting of the modes in we show in (b) the spin wave spectrum in a close vicinity of the Γ point. Now, the splitting and also gap in the spectrum are clearly visible.

the spin wave energy does not vanish at $k = 0$. This gap is a consequence of the in-plane easy-axis anisotropy, D_z , as shown in Fig.4a, where the two modes at the Γ point are plotted as a function of D_z . When $D_z = 0$, energy of the lowest mode vanishes, while the gap between the two modes survives. This gap, in turn, is determined mainly by the easy plane anisotropy constant, as shown in Fig.4b.

As we have already discussed above, external magnetic field leads to spin reorientation in the two monolayers. The transition to spin-flop phase appears at h_{sf} and then at the saturation field h_s the transition to fully collinear (ferromagnetic) phase takes place. The threshold fields h_s and h_{sf} are determined by the anisotropy constants and interlayer exchange parameter, as described in section 2. Variation of the the fields h_s and h_{sf} with the easy-axis anisotropy constant D_z is shown in Fig.5. To present a complete physical picture, we plot there h_s

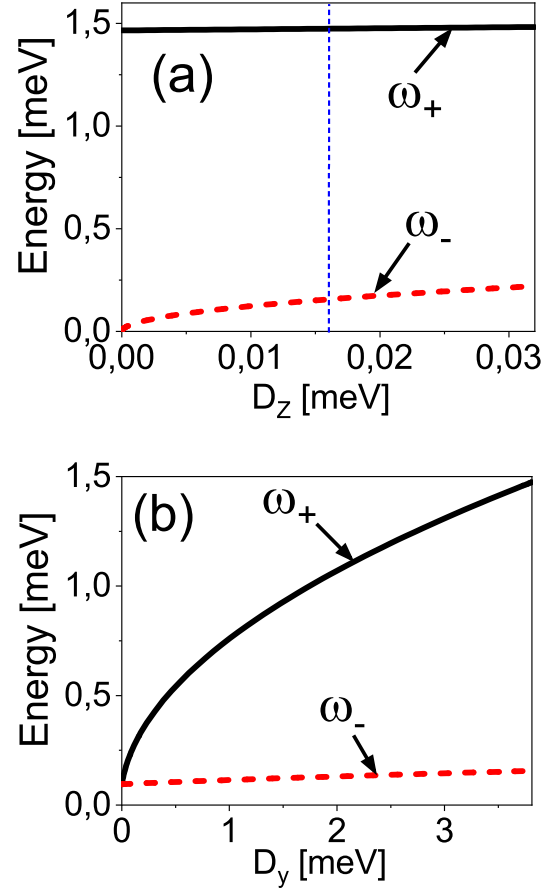


FIG. 4. Energy of the two modes in the Γ point as a function of (a) the in-plane easy-axis anisotropy constant D_z (the blue dashed line indicates D_z used for VTe₂ system), and (b) as a function of the easy-plane magnetic anisotropy constant D_y .

and h_{sf} for D_z significantly exceeding the value of D_z in 2H-VTe₂, while the other parameters correspond to 2H-VTe₂. This figure shows that when $D_z = 0$, the transition to the spin-flop phase appears already at infinitesimally small magnetic field. This figure also shows that in a general case the saturation field decreases with increasing D_z and for a specific value of D_z (denoted as D_z^M) the saturation field and the transition field to the spin-flop phase become equal, and the system changes from antiferromagnetic to ferromagnetic without the intermediate spin-flop phase (so-called metamagnetic transition). However, this does not happen in 2H-VTe₂ due to a small value of D_z in this material, indicated by the vertical dashed line in Fig.5. Accordingly, transition to the spin-flop phase takes place at a small magnetic field, and the range of magnetic field where the antiparallel configuration is stable is very narrow. In turn, the range of magnetic field with stable spin-flop phase is relatively large. This is shown explicitly in Fig.6, where the dispersion curves are plotted as a function of external magnetic

field.

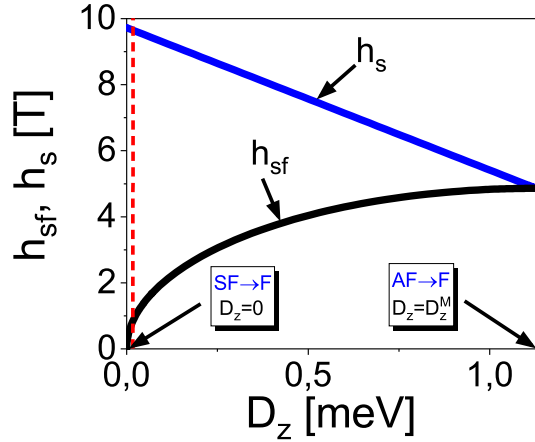


FIG. 5. The spin-flop field h_{sf} and saturation field h_s , plotted as a function of in-plane easy-axis anisotropy constant D_z . The range of D_z in this figure covers the full range where the spin-flop phase may appear, i.e. from $D_z = 0$ to D_z where a metamagnetic transition occurs. The vertical dashed line corresponds to D_z in VTe₂, which indicates that the range of magnetic field where the antiparallel state exist is very narrow, while the range of field with stable spin-flop phase is relatively broad. Note, the field units are here converted from energy units to Tesla.

Variation of the spin wave energy at the Γ point with increasing external magnetic field is shown in Fig.6a, while the same for the M and K points is shown in Fig.6b and Fig.6c, respectively. Note, that the two modes (black and red curves), behave differently in the three regions of magnetic field. In the antiferromagnetic phase, energy of one of the modes (that of higher energy) slightly increases with the field, whereas the second mode (of lower energy) becomes softened and reaches a minimum at the transition point to the spin-flop phase. This minimum is nonzero due to a finite in-plane easy-axis anisotropy. Slightly above the spin-flop field h_{sf} , energy of the lower mode (the soft one) increases with the field h , while energy of the upper mode decreases with increasing h . This tendency is kept till the saturation field h_s , where the latter modes becomes soft and its energy vanishes at h_s , while the energy of the former mode still increases with h for $h > h_s$, however a clear kink appears at the transition between the spin-flop and ferromagnetic phases. Similar behavior of the spin waves in the K and M points of the Brillouin zone is shown in Fig.6b and Fig.6c. In the antiferromagnetic phase one mode increase linearly with magnetic field, while the other decrease linearly with h . This is valid for both, K and M points. Interestingly, the two modes in the K point are degenerate in the spin-flop phase as well as in the ferromagnetic phase.

We note that some features of the spinwave spectra are similar to those found in spinwave spectra of artificially layered structures with antiferromagnetic interlayer cou-

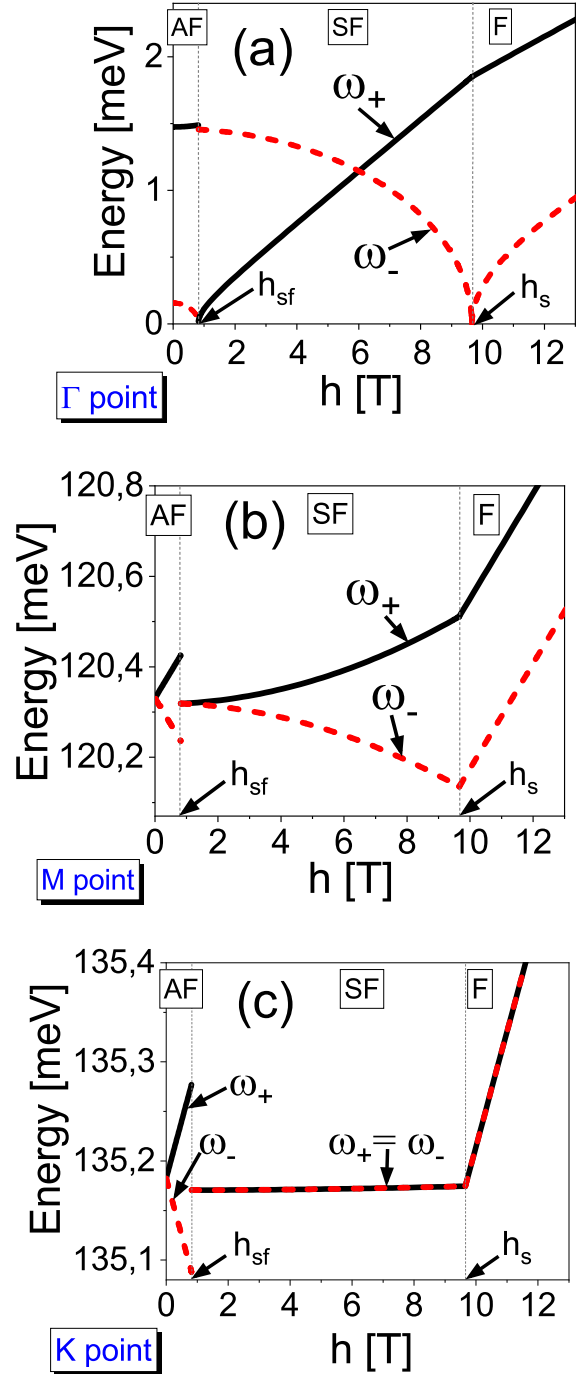


FIG. 6. Magnetic field (h) dependence of the spin wave spectra in the Γ (a), M (b), and K (c) points of the Brillouin zone. With increasing h , system goes from antiferromagnetic (AF) state to the spin-flop (SF) state at $h = h_{sf}$, and then from the spin-flop phase to the ferromagnetic (FM) state at $h = h_s$. Note, the field units are here converted from energy units to Tesla.

pling. Magnetic and electronic transport properties of such structures were studied extensively in 80s and 90s,

and the efforts resulted in the discovery of giant magnetoresistance effect [42, 43], which follows from spin dependent scattering processes [44]. The magnetic van der Waals materials are also layered magnetic structures, but with atomically thin magnetic layers and no nonmagnetic spacing layers. Therefore, spinwave spectra in both types of materials, i.e., artificial and van der Waals layered magnetic structures, have some similarities, and this similarity is especially evident in microscopic calculations of spin waves in artificially layered systems, like in the paper by Nortemann *et al* [45]. In that paper, the authors considered a stack of magnetic layers that were coupled antiferromagnetically, and in each magnetic layer there was a cubic spin lattice. Including exchange interactions, dipolar coupling, and Zeeman energy in an external magnetic field, the authors evaluated the spinwave spectra using the linearized equation of motion technique. In our paper we consider the bilayer of Vanadium based dichalcogenides with antiferromagnetic coupling of the two monolayers, and spin lattice in individual monolayers is hexagonal as shown in Fig.1. We also include two anisotropies, easy-plane and easy-axis ones, and calculate spinwaves within a fully quantum mechanical approach based on the Hollstein-Primakoff transformation followed by the Bogoliubov transformation. Despite some differences in the systems and techniques, certain features of the spinwave spectra are qualitatively similar, including softening of one spinwave mode at the transition from the antiferromagnetic to the spin-flop phase and at the transition from spin-flop to parallel state. Finally, we mention that various models and approximations were used to calculate spinwaves in artificially layered structures, including microscopic and macroscopic descriptions, effective medium theory, and others [46, 47].

IV. SUMMARY

In this paper we have analyzed spin wave modes in a class of van der Waals magnetic materials, that includes transition-metal dichalcogenides. The description is limited to bilayers with easy plane anisotropy and ferromagnetic intralayer exchange coupling, i.e. individual monolayers are ferromagnetically ordered in the layer plane. In turn, the two layers are coupled either ferromagnetically or antiferromagnetically. To find the spin wave energy we used the Hollstein-Primakoff-Bogolubov diagonalization scheme.

The bilayers support two magnon modes, which are split in general, though the splitting is rather small due to small interlayer exchange coupling. In the absence of external magnetic field and in-plane easy-axis anisotropy, energy of one of the modes vanishes in the Γ point of the Brillouin zone. This mode is the well known Goldstone mode. External field or in-plane anisotropy create a gap at the Γ point.

Van der Waals materials are of current interest from the point of view of possible applications. But of par-

ticular interest are bilayers of van der Waals magnetic materials, that can be considered as natural atomically-thin spin valves.

ACKNOWLEDGMENTS

This work has been supported by the Norwegian Financial Mechanism 2014- 2021 under the Polish Norwegian Research Project NCN GRIEG 2Dtronics no. 2019/34/H/ST3/00515.

Appendix A: Spin phases

As already mentioned in the main text, for the model Hamiltonian (1) and (2) one may expect in general three stable spin configurations of the bilayer system in an external magnetic field applied along the in-plane easy axis, i.e. (i) antiferromagnetic state at low fields with the spins of the two monolayers oriented along $+z$ and $-z$ axis for the bottom and top layers, respectively, (ii) spin-flop phase in a specific range of magnetic field, with the spins of the two monolayers lying in the atomic planes at an angle χ to the z axis, (iii) and the ferromagnetic phase with the spins of both layers along the z axis. In order to determine these phases in a specific magnetic field (and also bearing in mind the magnon description) it is convenient to use coordinate systems with the local z' axes along the corresponding spin orientations. To do this one has to combine rotation of the spins from the global frame around the y -axis by the canting angle χ and around the z -axis by the angle θ_α , where $\alpha = T$ and $\alpha = B$ labels the top and bottom layers, respectively,

$$\mathbf{S}_{\mathbf{r},\alpha} = \hat{\mathbf{R}}_z(\theta_\alpha)\hat{\mathbf{R}}_y(\chi)\mathbf{S}'_{\mathbf{r},\alpha}, \quad (\text{A1})$$

where the rotation matrix reads

$$\hat{\mathbf{R}}_z(\theta_\alpha)\hat{\mathbf{R}}_y(\chi) = \begin{pmatrix} \cos\theta_\alpha \cos\chi & -\sin\theta_\alpha \cos\theta_\alpha \sin\chi & \\ \sin\theta_\alpha \cos\chi & \cos\theta_\alpha \sin\theta_\alpha \sin\chi & \\ -\sin\chi & 0 & \cos\chi \end{pmatrix}, \quad (\text{A2})$$

with $\theta_T = \pi$ for the top layer, $\theta_B = 0$ for the bottom layer, and χ being the polar angle between the spin (aligned along the z' -axis of the local coordinate system) and the z -axis of the global frame. Thus,

$$S_{\mathbf{r},\alpha}^x = \mp S'_{\mathbf{r},\alpha}{}^x \sin\chi \mp S'_{\mathbf{r},\alpha}{}^z \cos\chi, \quad (\text{A3})$$

$$S_{\mathbf{r},\alpha}^y = \mp S'_{\mathbf{r},\alpha}{}^y, \quad (\text{A4})$$

$$S_{\mathbf{r},\alpha}^z = -S'_{\mathbf{r},\alpha}{}^x \cos\chi + S'_{\mathbf{r},\alpha}{}^z \sin\chi, \quad (\text{A5})$$

where the sign $-(+)$ corresponds to the layers $\alpha = T$ ($\alpha = B$), respectively.

The h - dependent regimes of the spin configurations of the bilayer can be found from the classical energy. In the

spin-flop phase, $h_{sf} \leq h \leq h_s$

$$E_{sf}/NS = -6|J_1|S + \xi J_2 S \cos 2\chi - \frac{1}{2}D_z S \cos^2 \chi - h \cos \chi, \quad (\text{A6})$$

where N is the total number of sites, and ξ denotes the structure factor: $\xi = 3$ and $\xi = 1$ for the H and T phase, respectively. Hence, minimizing the classical energy, $\partial E_{sf}/\partial \chi = 0$, yields the condition for the canting angle χ , $\cos \chi = h/h_s$, where h_s is the threshold magnetic field (the saturation field) at which the transition between spin-flop and ferromagnetic ($\chi = 0$) phases occurs,

$$h_s = S(4\xi J_2 - D_z). \quad (\text{A7})$$

The threshold h_{sf} for transition from the antiferromagnetic phase to the spin-flop one can be derived from the condition $E_{sf} = E_{af}$, where E_{af} denotes the classical energy for the collinear antiferromagnetic phase,

$$E_{af}/NS = -6|J_1|S - \xi J_2 S - \frac{1}{2}D_z S. \quad (\text{A8})$$

Thus, from Eqs. (A6) to (A8) one finds

$$h_{sf} = \sqrt{SD_z h_s} = S\sqrt{D_z(4\xi J_2 - D_z)}. \quad (\text{A9})$$

One can see that $h_{sf} = 0$ if $D_z = 0$. Thus, even for nonvanishing magnetic fields, $0 < h < h_{sf}$, the collinear antiferromagnetic configuration may exist as it is stabilized by the in-plane magnetic anisotropy.

Appendix B: Structural properties

For the considered VSe₂ system, each layer has hexagonal lattice with the primitive lattice vectors

$$\mathbf{a}_{1,2} = a \left(\pm \frac{\sqrt{3}}{2} \hat{\mathbf{x}} + \frac{1}{2} \hat{\mathbf{z}} \right), \quad \mathbf{a}_3 = 0, \quad (\text{B1})$$

where a is the in-plane lattice constant (distance between Vanadium atoms). Here, each V atom has six intralayer nearest neighbours determined by the $\boldsymbol{\delta}$ vectors:

$$\begin{aligned} \boldsymbol{\delta}_{1,2} &= \pm a \hat{\mathbf{z}}, \\ \boldsymbol{\delta}_{3,4} &= a \left(\pm \frac{\sqrt{3}}{2} \hat{\mathbf{x}} + \frac{1}{2} \hat{\mathbf{z}} \right), \\ \boldsymbol{\delta}_{5,6} &= a \left(\pm \frac{\sqrt{3}}{2} \hat{\mathbf{x}} - \frac{1}{2} \hat{\mathbf{z}} \right). \end{aligned} \quad (\text{B2})$$

Moreover, for the T-stacked system, each V atom has one NN in the adjacent layer, while for the H-stacked system there are three NNs in the adjacent layer with $\boldsymbol{\delta}$ given by

$$\boldsymbol{\delta}_{1,3} = a \left(-\frac{1}{2\sqrt{3}} \hat{\mathbf{x}} \pm \frac{1}{2} \hat{\mathbf{z}} \right), \quad \boldsymbol{\delta}_2 = \frac{a}{\sqrt{3}} \hat{\mathbf{x}}. \quad (\text{B3})$$

Appendix C: Holstein-Primakoff transformations in SF phase

Using the Holstein-Primakoff transformation, which for the SF configuration reads

$$S_{\mathbf{r},\alpha}^x = \sqrt{\frac{S}{2}} (a_{\mathbf{r},\alpha}^+ + a_{\mathbf{r},\alpha}), \quad (\text{C1})$$

$$S_{\mathbf{r},\alpha}^y = i\sqrt{\frac{S}{2}} (a_{\mathbf{r},\alpha}^+ - a_{\mathbf{r},\alpha}), \quad (\text{C2})$$

$$S_{\mathbf{r},\alpha}^z = S - a_{\mathbf{r},\alpha}^+ a_{\mathbf{r},\alpha}, \quad (\text{C3})$$

we arrive at the following form of the Hamiltonian written for the bosonic operators:

$$\begin{aligned} H &= J_1 S \sum_{\mathbf{r},\delta,\alpha} (a_{\mathbf{r},\alpha}^+ a_{\mathbf{r}+\delta,\alpha} + a_{\mathbf{r}+\delta,\alpha}^+ a_{\mathbf{r},\alpha} - a_{\mathbf{r},\alpha}^+ a_{\mathbf{r},\alpha} - a_{\mathbf{r}+\delta,\alpha}^+ a_{\mathbf{r}+\delta,\alpha}) \\ &+ 2J_2 S \sum_{\mathbf{r},\delta} \left[-\cos 2\chi (a_{\mathbf{r},T}^+ a_{\mathbf{r},T} + a_{\mathbf{r}+\delta,B}^+ a_{\mathbf{r}+\delta,B}) + \sin^2 \chi (a_{\mathbf{r},T}^+ a_{\mathbf{r}+\delta,B}^+ + a_{\mathbf{r},T} a_{\mathbf{r}+\delta,B}) \right. \\ &\left. - \cos^2 \chi (a_{\mathbf{r},T}^+ a_{\mathbf{r}+\delta,B} + a_{\mathbf{r},T} a_{\mathbf{r}+\delta,B}^+) \right] \\ &+ \frac{D_y S}{4} \sum_{\mathbf{r},\alpha} (2a_{\mathbf{r},\alpha}^+ a_{\mathbf{r},\alpha} - a_{\mathbf{r},\alpha}^+ a_{\mathbf{r},\alpha}^+ - a_{\mathbf{r},\alpha} a_{\mathbf{r},\alpha}) \\ &+ \frac{D_z S}{2} \sum_{\mathbf{r},\alpha} \left[(3 \cos^2 \chi - 1) a_{\mathbf{r},\alpha}^+ a_{\mathbf{r},\alpha} - \frac{1}{2} \sin^2 \chi (a_{\mathbf{r},\alpha}^+ a_{\mathbf{r},\alpha}^+ + a_{\mathbf{r},\alpha} a_{\mathbf{r},\alpha}) \right] \\ &+ h \cos \chi \sum_{\mathbf{r},\alpha} a_{\mathbf{r},\alpha}^+ a_{\mathbf{r},\alpha}. \end{aligned} \quad (\text{C4})$$

The Fourier transformation described by Eq. (9) together with Eqs. (B1)-(B3) yields

$$\begin{aligned} H &= \sum_{\mathbf{k}} \left\{ 2J_1 S \sum_{\alpha} (\gamma_{\mathbf{k}} - 6) a_{\mathbf{k},\alpha}^+ a_{\mathbf{k},\alpha} + 2J_2 S \left[-\xi \cos 2\chi \sum_{\alpha} a_{\mathbf{k},\alpha}^+ a_{\mathbf{k},\alpha} + \sin^2 \chi (\eta_{\mathbf{k}} a_{-\mathbf{k},T}^+ a_{\mathbf{k},B}^+ + \eta_{\mathbf{k}}^* a_{-\mathbf{k},T} a_{\mathbf{k},B}) \right. \right. \\ &\left. \left. - \cos^2 \chi (\eta_{\mathbf{k}}^* a_{\mathbf{k},T}^+ a_{\mathbf{k},B} + \eta_{\mathbf{k}} a_{\mathbf{k},T} a_{\mathbf{k},B}^+) \right] + \frac{S}{2} \sum_{\alpha} \left\{ \left[D_y + D_z (3 \cos^2 \chi - 1) \right] a_{\mathbf{k},\alpha}^+ a_{\mathbf{k},\alpha} - \frac{1}{2} (D_y + D_z \sin^2 \chi) (a_{\mathbf{k},\alpha}^+ a_{-\mathbf{k},\alpha}^+ + a_{\mathbf{k},\alpha} a_{-\mathbf{k},\alpha}) \right\} \right. \\ &\left. + h \cos \chi \sum_{\alpha} a_{\mathbf{k},\alpha}^+ a_{\mathbf{k},\alpha} \right\}, \end{aligned} \quad (\text{C5})$$

which within the Bogolubov transformation approach leads to the final form of the Hamiltonian $H = H_{\mathbf{k}} + H_{-\mathbf{k}}$, where $H_{\mathbf{k}}$ is given by Eq.(33) in the main text.

Appendix D: Ferromagnetic interlayer coupling

If the TMD 2H-VX₂ bilayer has FM ground state (as e.g. 2H-VS₂), then Eq. (3) describes ferromagnetic interlayer coupling with exchange coupling parameter $J_2 < 0$. In such a case the Holstein-Primakoff and Fourier transformations for the top and bottom layers lead to the full Hamiltonian in the form

$$\begin{aligned}
 H = \sum_{\mathbf{k}} \left\{ 2J_1 S \sum_{\alpha} (\gamma_{\mathbf{k}} - 6) a_{\mathbf{k},\alpha}^+ a_{\mathbf{k},\alpha} \right. \\
 + 2J_2 S \left(-\xi \sum_{\alpha} a_{\mathbf{k},\alpha}^+ a_{\mathbf{k},\alpha} + \eta_{\mathbf{k}} a_{\mathbf{k},T} a_{\mathbf{k},B}^+ + \eta_{\mathbf{k}}^* a_{\mathbf{k},T}^+ a_{\mathbf{k},B} \right) \\
 + S \sum_{\alpha} \left[-\frac{D_y}{4} (a_{\mathbf{k},\alpha}^+ a_{-\mathbf{k},\alpha}^+ + a_{\mathbf{k},\alpha} a_{-\mathbf{k},\alpha} - 2a_{\mathbf{k},\alpha}^+ a_{\mathbf{k},\alpha}) \right. \\
 \left. \left. + D_z a_{\mathbf{k},\alpha}^+ a_{\mathbf{k},\alpha} \right] + h \sum_{\alpha} a_{\mathbf{k},\alpha}^+ a_{\mathbf{k},\alpha} \right\}. \quad (D1)
 \end{aligned}$$

The eigenvalue problem evaluated by means of the Bogolubov diagonalization scheme leads finally to the dispersion relation given by the formula

$$\omega_{\mathbf{k},\mu} = \left[(A_{\mathbf{k}} \pm |B_{\mathbf{k}}|)^2 - 4C^2 \right]^{\frac{1}{2}}, \quad (D5)$$

where $A_{\mathbf{k}}$ and $|B_{\mathbf{k}}|$ are given by Eq. (D4) (note that here $|B_{\mathbf{k}}| \equiv |\tilde{B}_{\mathbf{k}}|$), and where \pm corresponds to mode $\mu = +, -$. At the zone center, $\mathbf{k} = 0$, one gets

$$\omega_{\mathbf{k}=0,+} = S \left[\left(12|J_2| + \frac{D_y}{2} + D_z \right)^2 - \left(\frac{D_y}{2} \right)^2 \right]^{\frac{1}{2}} \quad (D6)$$

This Hamiltonian can be written as

$$H = H_{\mathbf{k}} + H_{-\mathbf{k}}, \quad (D2)$$

where

$$\begin{aligned}
 H_{\mathbf{k}} = \sum_{\mathbf{k}} \left[\sum_{\alpha} \left(\frac{A_{\mathbf{k}}}{2} \right) a_{\mathbf{k},\alpha}^+ a_{\mathbf{k},\alpha} + B_{\mathbf{k}} a_{\mathbf{k},T}^+ a_{\mathbf{k},B} \right. \\
 \left. + C \sum_{\alpha} a_{\mathbf{k},\alpha} a_{-\mathbf{k},\alpha} \right] + H.c., \quad (D3)
 \end{aligned}$$

with

$$\begin{aligned}
 A_{\mathbf{k}} &= S \left[2J_1 (\gamma_{\mathbf{k}} - 6) - 2\xi J_2 + \frac{D_y}{2} + D_z \right] + h, \\
 B_{\mathbf{k}} &= 2\eta_{\mathbf{k}}^* J_2 S, \\
 C &= -\frac{D_y S}{4}. \quad (D4)
 \end{aligned}$$

so that in the absence of the Zeeman field ($h = 0$) as well as in the absence of the in-plane anisotropy field ($D_z = 0$), one finds $\omega_{\mathbf{k}=0,-} = 0$. In such a case, for $D_y > 0$ a gapless, linearly vanishing $\sim |\mathbf{k}|$ Goldstone mode occurs at the zone center, while for $D_y = 0$ the mode $\omega_{\mathbf{k},-}$ vanishes non-linearly in the vicinity of $\mathbf{k} = 0$.

-
- [1] K.S. Burch, D. Mandrus, and J.G. Park, *Magnetism in two-dimensional van der Waals materials*, [Nature](#) **563**, 47 (2018)
- [2] Q. H. Wang, et al., *The Magnetic Genome of Two-Dimensional van der Waals Materials*, [ACS Nano](#) **16**, 6960 (2022)
- [3] Y. Li, B. Yang, S. Xu, B. Huang, and W. Duan, *Emergent Phenomena in Magnetic Two-Dimensional Materials and van der Waals Heterostructures*, [ACS Appl. Electron. Mater.](#) **4**, 3278 (2022)
- [4] M. A. Jafari et al, *Spin valve effect in two-dimensional VSe₂ system*, [Journal of Magn. Magn. Materials](#) **548**, 168921 (2022).
- [5] S. Dasgupta and O. Tchernyshyov, *Theory of spin waves in a hexagonal antiferromagnet*, [Phys. Rev. B](#) **102**, 144417 (2020).
- [6] S. S. Pershoguba, S. Banerjee, C. Lashley, J. Park, H. gren, G. Aeppli, and A. V. Balatsky, *Dirac Magnons in Honeycomb Ferromagnets*, [Physical Review X](#) **8**, 011010 (2018)
- [7] A. Jain, M. Krautloher, J. Porras, G. H. Ryu, D. P. Chen, D. L. Abernathy, J. T. Park, A. Ivanov, J. Chaloupka, G. Khaliullin, B. Keimer, and B. J. Kim, *Higgs mode and its decay in a two-dimensional antiferromagnet* [Nature Physics](#) **13**, 633, (2017)
- [8] L. Chen, J.-H. Chung, B. Gao, T. Chen, M. B. Stone, A. I. Kolesnikov, Q. Huang, and P. Dai, *Topological Spin Excitations in Honeycomb Ferromagnet CrI₃*, [Physical Review X](#) **8**, 041028 (2018)
- [9] A.T. Costa, D. L. R. Santos, N. M. R. Peres, and J. Fernandez-Rossier, *Topological magnons in CrI₃ monolayers: an itinerant fermion description*, [2D Mater.](#) **7**, 045031 (2020)
- [10] L. C. Ortmann, G. E. W. Bauer, and Y. M. Blanter, *Magnon dispersion in bilayers of two-dimensional ferromagnets*, [Physical Review B](#) **103**, 155430 (2021)

- [11] D. Ghader, *Insights on magnon topology and valley-polarization in 2D bilayer quantum magnets*, *New Journal of Physics*, **23**, 053022 (2021).
- [12] Z.-W. Lu, et al., *Theoretical Study of Strain Induced Magnetic Transition of Single-Layer CrTe₃*, *J. Appl. Phys.* **127**, 033903 (2020)
- [13] Q. Cui, et al., *Strain-Tunable Ferromagnetism and Chiral Spin Textures in Two-Dimensional Janus Chromium Dichalcogenides*; *Phys. Rev. B* **102**, 094425 (2020)
- [14] I. A. Verzhbitskiy, et al., *Controlling the Magnetic Anisotropy in Cr₂Ge₂Te₆ by Electrostatic Gating*, *Nature Electronics* **3**, 460 (2020)
- [15] C. Tan, et al., *Gate-Controlled Magnetic Phase Transition in a van der Waals Magnet Fe₅GeTe₂*, *Nano Lett.* **21**, 5599 (2021)
- [16] K. OGrady, J. Sinclair, K. Elphick, R. Carpenter, G. Vallejo-Fernandez, M. I. J. Probert, and A. Hirohata, *Anisotropy in antiferromagnets*, *Journal of Applied Physics* **128**, 040901 (2020).
- [17] F. Li, K. Tu, and Z. Chen, *Versatile Electronic Properties of VSe₂ Bulk, Few-Layers, Monolayer, Nanoribbons, and Nanotubes: A Computational Exploration*, *J. Phys. Chem. C* **118**, 21264 (2014).
- [18] H.-R. Fuh, B. Yan, S.-Ch. Wu, C. Felser and Ch.-R. Chang, *Metal-insulator transition and the anomalous Hall effect in the layered magnetic materials VS₂ and VSe₂*, *New Journal of Physics* **18**, 113038 (2016).
- [19] H.-R. Fuh, Ch.-R. Chang, Y.-K. Wang, R. F. L. Evans, R. W. Chantrell and H.-T. Jeng, *Newtype single-layer magnetic semiconductor in transition-metal dichalcogenides VX₂ (X=S, Se and Te)*, *Scientific Reports* **6**, 32625 (2016).
- [20] S.-J. Gong, Ch. Gong, Y.-Y. Sun, W.-Y. Tong, Ch.-G. Duan, J.-H. Chu and X. Zhang, *Electrically induced 2D half-metallic antiferromagnets and spin field effect transistors*, *PNAS* **115**, 8511 (2018).
- [21] Q. Jiang, W. Xia, T. Xu, W. Liu, X. Shen, Y. Guo, M. Ye and S. Qiao, *Independent spin polarized valence electronic states in VSe₂ from charge density wave transition*, *Journal of Electron Spectroscopy and Related Phenomena* **238**, 146868 (2020).
- [22] Ø. Johansen, V. Risinggård, A. Sudbø, J. Linder and A. Brataas, *Current Control of Magnetism in Two-Dimensional Fe₃GeTe₂*, *Phys. Rev. Lett.* **122**, 217203 (2019).
- [23] B. Huang, et al., *Layer-dependent ferromagnetism in a van der Waals crystal down to the monolayer limit*, *Nature* **546**, 270 (2017); DOI: 10.1038/nature22391
- [24] C. Gong, L. Li, Z. Li, H. Ji, A. Stern, Y. Xia, T. Cao, W. Bao, C. Wang, Y. Wang, Z. Q. Qiu, R. J. Cava, S. G. Louie, J. Xia, and X. Zhang, *Discovery of intrinsic ferromagnetism in two-dimensional van der Waals crystals*, *Nature* **546**, 265 (2017)
- [25] M. Chhowalla, H. S. Shin, G. Eda, L.-J. Li, K. P. Loh, and H. Zhang, *The chemistry of two-dimensional layered transition metal dichalcogenide nanosheets*, *Nat. Chemistry* **5**, 263 (2013).
- [26] J. Feng, X. Sun, Ch. Wu, L. Peng, Ch. Lin, S. Hu, J. Yang, and Y. Xie, *Metallic Few-Layered VS₂ Ultrathin Nanosheets: High Two-Dimensional Conductivity for In-Plane Supercapacitors*, *J. Am. Chem. Soc.* **133**, 44, 17832 (2011).
- [27] H. Zhang, M.-L. Liu, and W. M. Lau, *Dimension-dependent phase transition and magnetic properties of VS₂*, *J. Mater. Chem. A*, **1**, 10821 (2013).
- [28] M. Bayard and M.J.Sienko, *Anomalous electrical and magnetic properties of vanadium diselenide*, *Journal of Solid State Chemistry* **19**, 325 (1976).
- [29] G. Aivazian, Z. Gong, A. M. Jones, R.-L. Chu, J. Yan, D. G. Mandrus, C. Zhang, D. Cobden, W. Yao and X. Xu, *Magnetic control of valley pseudospin in monolayer WSe₂*, *Nature Physics* **11**, 148 (2015).
- [30] D. MacNeill, C. Heikes, K. F. Mak, Z. Anderson, A. Kormnyos, V. Zlyomi, J. Park and D. C. Ralph, *Breaking of Valley Degeneracy by Magnetic Field in Monolayer MoSe₂*, *Phys. Rev. Lett.* **114**, 037401 (2015).
- [31] W. Zhao, B. Dong, Z. Guo, G. Su, R. Gao, W. Wanga and L. Cao, *Colloidal synthesis of VSe₂ single-layer nanosheets as novel electrocatalysts for the hydrogen evolution reaction*, *Chem. Commun.* **52**, 9228 (2016).
- [32] A. Kamra, U. Agrawal, and W. Belzig, *Noninteger-spin magnonic excitations in untextured magnets*, *Physical Review B* **96**, 020411(R) (2017)
- [33] G. Engelhardt and T. Brandes, *Topological Bogoliubov excitations in inversion-symmetric systems of interacting bosons*, *Phys. Rev. A* **91**, 053621 (2015).
- [34] S. A. Owerre, *Magnonic Floquet Quantum Spin Hall Insulator in Bilayer Collinear Antiferromagnets*, *Scientific Reports* **9**, 7197 (2019).
- [35] M. Abdollahi and M. B. Tagani, *Tuning the magnetic properties of a VSe₂ monolayer via the magnetic proximity effect mediated by Zeeman type spin-orbit interaction*, *Phys. Rev. B* **108**, 024427 (2023).
- [36] J. Liu; H.-J. Koo; H. Xiang; R. K. Kremer; M.-H. Whangbo, *Most spin-1/2 transition-metal ions do have single ion anisotropy*, *J. Chem. Phys.* **141**, 124113 (2014).
- [37] X. Wang, D. Li, Z. Li, C. Wu, G. Chen, X. Cui, *Ferromagnetism in 2D Vanadium Diselenide*, *ACS Nano*, **15**, 10, 16236 (2021).
- [38] M. Esters, R. G. Hennig, D. C. Johnson, *Dynamic instabilities in strongly correlated VSe₂ Monolayers and bilayers*, *Phys. Rev. B* **96**, 235147 (2017).
- [39] G. Liu, H. Jiang, Z. Guo, X. Zhang, L. Jin, C. Liu, Y. Liu, *Magnetic second-order topological insulators in 2H-transition metal dichalcogenides*, *Advanced Science*, **2301952**, (2023).
- [40] S. Feng, W. Mi, *Strain and interlayer coupling tailored magnetic properties and valley splitting in layered ferrovalley 2H-VSe₂*, *Appl. Surf. Sci.* **458**, 191 (2018).
- [41] M. A. Jafari et al to be published
- [42] M. N. Baibich, J. M. Broto, A. Fert, F. Nguyen Van Dau, F. Petroff, P. Etienne, G. Creuzet, A. Friederich, and J. Chazelas, *Giant Magnetoresistance of (001)Fe/(001)Cr Magnetic Superlattices*, *Phys. Rev. Lett.* **61**, 2472 (1988).
- [43] G. Binash, P. Grünberg, F. Saurenbach, and W. Zinn, *Enhanced magnetoresistance in layered magnetic structures with antiferromagnetic interlayer exchange*, *Phys. Rev. B* **39**, 4828 (1989).
- [44] R. E. Camley and J. Barnas, *Theory of giant magnetoresistance effects in magnetic layered structures with antiferromagnetic coupling*, *Phys. Rev. Lett.* **63**, 664 (1989).
- [45] F. C. Nörtemann, R.L. Stamps, R.E. Camley, *Microscopic calculations of spin waves in antiferromagnetically coupled multilayers: Nonreciprocity and finite-size effects*, *Physical Review B* **47**, 11 910 (1993).
- [46] F. C. Nörtemann, R. L. Stamps, R. E. Camley, B. Hillebrands, and G. Güntherodt *Effective-medium theory for finite magnetic multilayers: Effect of anisotropy on dipole*

lar modes, *Phys. Rev. B* 47, 3225 (1993).

[47] J Barnaś, P. Grünberg, *Spin waves in exchange-coupled epitaxial double layers*, *J. Magn. Magn. Materials* 82, 186 (1989).